

Tensor bispectrum mediated by an excited scalar field during inflation

Zhi-Zhang Peng^{1,2,3,*}, Cheng-Jun Fang^{2,3,†} and Zong-Kuan Guo^{2,3,4‡}

¹*School of Physics and Astronomy, Beijing Normal University, Beijing 100875, People's Republic of China*

²*CAS Key Laboratory of Theoretical Physics, Institute of Theoretical Physics, Chinese Academy of Sciences, P.O. Box 2735, Beijing 100190, China*

³*School of Physical Sciences, University of Chinese Academy of Sciences, No.19A Yuquan Road, Beijing 100049, China and*

⁴*School of Fundamental Physics and Mathematical Sciences, Hangzhou Institute for Advanced Study, University of Chinese Academy of Sciences, Hangzhou 310024, China*

We calculate the tensor bispectrum mediated by an excited scalar field during inflation and find that the bispectrum peaks in the squeezed configuration, which is different from that of gravitational waves induced by enhanced curvature perturbations re-entering the horizon in the radiation-dominated era. Measuring the bispectrum provides a promising way to distinguish the stochastic gravitational-wave background generated during inflation from that generated after inflation.

I. INTRODUCTION

Recently, several pulsar timing array collaborations, including NANOGrav [1, 2], PPTA [3, 4], EPTA [5, 6] and CPTA [7], have individually reported the first compelling evidence for a stochastic gravitational-wave background (SGWB) signal. Such a SGWB signal is expected to arise from astrophysical sources or cosmological sources. Due to a mild tension between the astrophysical prediction of the spectral shape and the reconstructed one from observed data, cosmological sources fit current data better than astrophysical sources. If the signal is of cosmological origin, this raises a question: was the gravitational wave (GW) signal generated during inflation or after inflation?

For a Gaussian SGWB, regardless of its astrophysical or cosmological origin, the statistical properties of GWs is described only by the power spectrum, which depends on the generation mechanism of GWs. Distinguishing such a SGWB signal from various sources relies on detailed study of the power spectrum shape. Unfortunately, current pulsar timing array observations provide only weak constraints on the shape of the power spectrum, so that it is hard to identify the origin of the observed signal [8]. Actually, the interactions of quantum fields during inflation result in a large amount of non-Gaussianity of the SGWB. In this case, measurements of the power spectrum alone have limited potential in revealing the interactions during inflation. Compared to the power spectrum, the tensor bispectrum provides richer physical information and thus is expected to break the degeneracy of the GW sources.

In this paper, we calculate for the first time the one-loop tensor bispectrum mediated by an excited scalar field during inflation. It is known that the enhancement of the scalar field perturbation during inflation generically gives rise to two SGWBs [9–15]. One is sourced

by the enhanced scalar field perturbation and stretched to super-horizon scales during inflation. The other is produced when curvature perturbations enhanced during inflation re-enter the horizon in the radiation-dominated era. The relation for the peak amplitudes and peak frequencies in the spectrum of these two SGWBs is discussed in the specific models [10, 13] (see [16] for general discussion). Since the purpose of this work is to calculate the tensor bispectrum in the presence of the enhanced scalar field perturbation, we do not specify the mechanism to amplify the scalar field fluctuation but consider an exponential amplification of scalar modes during a short period of time.

Using the in-in formalism [17, 18], we compute the contribution of the one-loop diagrams, including the bubble and triangle diagrams, to the tensor bispectrum due to the interaction between the scalar field and tensor perturbations. Although the one-loop contribution is suppressed by a factor of H^2/M_p^2 where H is the Hubble parameter and M_p is the reduced Planck mass, the large enhancement of the scalar field perturbation can enable the loop contribution to be comparable to the tree-level (one-loop tensor power spectrum from an excited scalar field was first calculated in Refs. [19, 20], which also pointed out the implied large tensor non-Gaussianity.). Therefore, in this paper we focus on the calculation of the one-loop tensor bispectrum. Our results show that the tensor bispectrum mediated by an excited scalar field during inflation peaks in a squeezed configuration. Actually, the addition of the tree-level contribution to the bispectrum does not change this conclusion [17, 21, 22]. Such a shape of the bispectrum is different from that of the SGWB induced by enhanced curvature perturbations re-entering the horizon in the radiation-dominated era. It is found that the bispectrum of the latter is dominated by the equilateral configuration because the source of GWs is composed by gradients of curvature perturbations when re-entering the horizon [23, 24]. Measurements of the shape of the tensor bispectrum provide a promising way to distinguish the GW signal generated during inflation from that generated after inflation.

* pengzhizhang@bnu.edu.cn

† fangchengjun@itp.ac.cn

‡ guozk@itp.ac.cn

II. HIGHER ORDER ACTION

To expand the action to higher order in tensor perturbations, it is convenient to write the metric in the ADM form

$$ds^2 = -N^2 d\tau^2 + \gamma_{ij}(dx^i + N^i d\tau)(dx^j + N^j d\tau), \quad (1)$$

where N and N^i are the lapse function and shift vector, respectively, serving as Lagrange multipliers, τ is the conformal time, and γ_{ij} is the spatial components of the metric. Following Maldacena [17], we choose the following gauge to fix time and spatial reparametrizations around a spatially-flat Friedmann-Robertson-Walker metric, such that $N = a$, $N^i = 0$, and

$$\gamma_{ij} = a^2(\delta_{ij} + h_{ij} + \frac{1}{2}h_i^k h_{kj} + \frac{1}{6}h_i^k h_k^l h_{lj} + \dots), \quad (2)$$

where h_{ij} are tensor perturbations which are transverse ($\partial^i h_{ij} = 0$) and traceless ($\delta^{ij} h_{ij} = 0$).

We consider the loop contribution to the tensor bispectrum due to a minimally-coupled spectator scalar field χ . The scalar field fluctuation is denoted by $\delta\chi$. Then the action up to fourth order in h_{ij} and $\delta\chi$ is expanded as

$$S = M_p^2 \int d\tau d^3x a^2 \left(\frac{1}{4} h^{ik} h^{jl} - \frac{1}{8} h^{ij} h^{kl} \right) \partial_k \partial_l h_{ij} + \int d\tau d^3x a^2 \left(-\frac{1}{2} h^{ij} + \frac{1}{4} h^{ik} h_k^j \right) \partial_i \delta\chi \partial_j \delta\chi. \quad (3)$$

Then, Legendre transformation gives the interaction Hamiltonian

$$H_{\text{int}} = M_p^2 \int d^3x a^2 \left(-\frac{1}{4} h^{ik} h^{jl} + \frac{1}{8} h^{ij} h^{kl} \right) \partial_k \partial_l h_{ij} + \int d^3x a^2 \left(\frac{1}{2} h^{ij} - \frac{1}{4} h^{ik} h_k^j \right) \partial_i \delta\chi \partial_j \delta\chi. \quad (4)$$

Note that the terms in the first line in Eq. (4) represent the classical third-order gravitational Hamiltonian, which results in the tensor bispectrum dominated by the squeezed configuration [17, 21, 22]. The rest in Eq. (4) represent the interaction between $\delta\chi$ and h_{ij} which arise from the kinetic term of the minimally-coupled scalar field in the action. We shall focus on such a tensor-scalar interaction and calculate the tensor bispectrum mediated by the scalar field perturbation.

The Fourier modes of the scalar field perturbation and tensor perturbations are expressed as

$$\delta\chi(\tau, \mathbf{x}) = \int \frac{d^3k}{(2\pi)^3} e^{i\mathbf{k}\cdot\mathbf{x}} \delta\chi_{\mathbf{k}}(\tau), \quad (5)$$

$$h_{ij}(\tau, \mathbf{x}) = \int \frac{d^3k}{(2\pi)^3} e^{i\mathbf{k}\cdot\mathbf{x}} \sum_{s=\pm 2} e_{ij}^s(\mathbf{k}) h_{\mathbf{k}}^s(\tau), \quad (6)$$

where $e_{ij}^s(\mathbf{k})$ is the polarization tensor with the helicity states $s = \pm 2$, satisfying $e_{ij}^{s_1}(\mathbf{k}) e^{ij, s_2^*}(\mathbf{k}) = \delta^{s_1 s_2}$

and $e_{ij}^s(-\mathbf{k}) = e_{ij}^{s*}(\mathbf{k})$. The quantized field operators are expanded into the creation and annihilation operators as $\delta\chi_{\mathbf{k}}(\tau) = u_{\mathbf{k}}(\tau) a_{\mathbf{k}} + u_{\mathbf{k}}^*(\tau) a_{-\mathbf{k}}^\dagger$ and $h_{\mathbf{k}}^s(\tau) = v_{\mathbf{k}}(\tau) b_{\mathbf{k}}^s + v_{\mathbf{k}}^*(\tau) b_{-\mathbf{k}}^{s\dagger}$. The non-vanishing commutation relations for the creation and annihilation operators are given by $[a_{\mathbf{k}_1}, a_{-\mathbf{k}_2}^\dagger] = (2\pi)^3 \delta(\mathbf{k}_1 + \mathbf{k}_2)$ and $[b_{\mathbf{k}_1}^{s_1}, b_{-\mathbf{k}_2}^{s_2\dagger}] = (2\pi)^3 \delta^{s_1 s_2} \delta(\mathbf{k}_1 + \mathbf{k}_2)$. The initial conditions for the mode functions, $u_{\mathbf{k}}$ and $v_{\mathbf{k}}$, correspond to the Bunch-Davis vacuum, which are given by

$$u_{\mathbf{k}}^{\text{BD}}(\tau) = \frac{H}{\sqrt{2k^3}} (1 + ik\tau) e^{-ik\tau}, \quad (7)$$

$$v_{\mathbf{k}}^{\text{BD}}(\tau) = \frac{2H}{M_p \sqrt{2k^3}} (1 + ik\tau) e^{-ik\tau}. \quad (8)$$

III. TENSOR BISPECTRUM

Using the in-in formalism [17, 18], we compute the one-loop contribution to the tensor bispectrum from the gravitational interaction with the excited scalar field. The in-in formalism was firstly proposed by Maldacena to compute the non-Gaussianity of primordial tensor perturbations in the context of single-field slow-roll inflation [17, 21] and was later applied to extra fields [25, 26], non-attractor phase for tensor fluctuations [27], massive gravity theory [28], generalized G-inflation [22, 29–31], α -vacuum [32, 33], axion-gauge field models [34, 35], and more generally, effective field theory [36–39]. The equal-time correlators are computed with the in-in formalism via the following formula

$$\langle \mathcal{O} \rangle = \lim_{\tau_0 \rightarrow -\infty(1-i\epsilon)} \langle 0 | \bar{T} \exp \left(i \int_{\tau_0}^{\tau} d\tau' H_{\text{int}, I}(\tau') \right) \times \mathcal{O}_I(\tau) T \exp \left(-i \int_{\tau_0}^{\tau} d\tau'' H_{\text{int}, I}(\tau'') \right) | 0 \rangle, \quad (9)$$

where the subscript I labels fields in the interaction picture, T and \bar{T} denote the time and anti-time ordering operator, respectively. According to the order counting

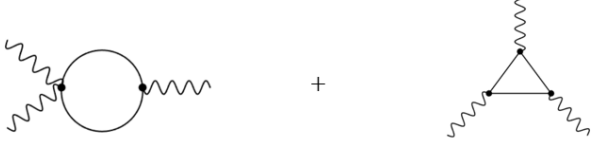


FIG. 1. One-loop Feynman diagrams including the bubble (*left*) and triangle (*right*) diagrams.

parameter, Eq. (9) is expanded to

$$\langle \mathcal{O} \rangle_0 = \langle 0 | \mathcal{O}_I(\tau) | 0 \rangle, \quad (10)$$

$$\langle \mathcal{O} \rangle_1 = 2 \text{Im} \int_{\tau_0}^{\tau} d\tau' \langle 0 | \mathcal{O}_I(\tau) H_{\text{int},I}(\tau') | 0 \rangle, \quad (11)$$

$$\begin{aligned} \langle \mathcal{O} \rangle_{2a} &= \int_{\tau_0^*}^{\tau} d\tau' \int_{\tau_0}^{\tau} d\tau'' \\ &\times \langle 0 | H_{\text{int},I}(\tau') \mathcal{O}_I(\tau) H_{\text{int},I}(\tau'') | 0 \rangle, \end{aligned} \quad (12)$$

$$\begin{aligned} \langle \mathcal{O} \rangle_{2b} &= -2 \text{Re} \int_{\tau_0}^{\tau} d\tau' \int_{\tau_0}^{\tau'} d\tau'' \\ &\times \langle 0 | \mathcal{O}_I(\tau) H_{\text{int},I}(\tau') H_{\text{int},I}(\tau'') | 0 \rangle, \end{aligned} \quad (13)$$

$$\begin{aligned} \langle \mathcal{O} \rangle_{3a} &= 2 \text{Im} \int_{\tau_0}^{\tau} d\tau' \int_{\tau_0}^{\tau'} d\tau'' \int_{\tau_0}^{\tau''} d\tau''' \\ &\times \langle 0 | H_{\text{int},I}(\tau') \mathcal{O}_I(\tau) H_{\text{int},I}(\tau'') H_{\text{int},I}(\tau''') | 0 \rangle, \end{aligned} \quad (14)$$

$$\begin{aligned} \langle \mathcal{O} \rangle_{3b} &= -2 \text{Im} \int_{\tau_0^*}^{\tau} d\tau' \int_{\tau_0}^{\tau'} d\tau'' \int_{\tau_0}^{\tau''} d\tau''' \\ &\times \langle 0 | \mathcal{O}_I(\tau) H_{\text{int},I}(\tau') H_{\text{int},I}(\tau'') H_{\text{int},I}(\tau''') | 0 \rangle, \end{aligned} \quad (15)$$

with $\langle \mathcal{O} \rangle_2 \equiv \langle \mathcal{O} \rangle_{2a} + \langle \mathcal{O} \rangle_{2b}$ and $\langle \mathcal{O} \rangle_3 \equiv \langle \mathcal{O} \rangle_{3a} + \langle \mathcal{O} \rangle_{3b}$. Since the vacuum expectation values of \mathcal{O} are evaluated at the end of inflation, we set $\tau = 0$ in the end of calculation. For the three-point correlators of GWs, $\langle \mathcal{O} \rangle_0$ vanishes. Given the interaction Hamiltonian (4), we can calculate the vacuum expectation value of the three-point correlators $\langle \mathcal{O} \rangle_1$, $\langle \mathcal{O} \rangle_2$ and $\langle \mathcal{O} \rangle_3$. The first one is the tree-level contribution while $\langle \mathcal{O} \rangle_2$ and $\langle \mathcal{O} \rangle_3$ are the one-loop contributions, which correspond to the bubble (left) and triangle (right) Feynman diagrams in Fig. 1, respectively. Eqs. (12)-(15) are the basic equations we use in what follows.

Traditionally, to capture the shape of the tensor bispectrum it is convenient to define the shape function $S^{s_1 s_2 s_3}(k_1, k_2, k_3)$ by

$$\begin{aligned} \langle h_{\mathbf{k}_1}^{s_1}(\tau) h_{\mathbf{k}_2}^{s_2}(\tau) h_{\mathbf{k}_3}^{s_3}(\tau) \rangle &= (2\pi)^3 \delta(\mathbf{k}_1 + \mathbf{k}_2 + \mathbf{k}_3) \\ &\times \frac{\mathcal{P}_h^2}{k_1^2 k_2^2 k_3^2} S^{s_1 s_2 s_3}(k_1, k_2, k_3), \end{aligned} \quad (16)$$

where \mathcal{P}_h is the power spectrum of tensor perturbations given by $\mathcal{P}_h = \frac{2H^2}{\pi^2 M_{\text{p}}^2}$ in the slow-roll inflationary model. The amplitude of the bispectrum relies on the amplification factor of the scalar field perturbation. In this work, we are interested in the shape of the bispectrum

rather than its amplitude. Since the one-loop contribution is suppressed by a factor of H^2/M_{p}^2 , we rescale the shape function as $\langle h_{\mathbf{k}_1}^{s_1} h_{\mathbf{k}_2}^{s_2} h_{\mathbf{k}_3}^{s_3} \rangle' (H/M_{\text{p}})^{-6} k_1^2 k_2^2 k_3^2$, where the prime denotes omitting the delta function for the momentum conservation.

IV. ONE-LOOP CONTRIBUTIONS FROM THE EXCITED SCALAR FIELD

We consider an exponential growth of the scalar field perturbation on sub-horizon scales, which can be achieved through parametric resonance [9–15]. The amplification of $\delta\chi$ from t_i to t_f is given by $\delta\chi = e^{\mu H(t_f - t_i)} \delta\chi_{\text{BD}}$, where μ is a dimensionless constant. In terms of the conformal time, the amplification factor $\mathcal{A} = e^{\mu H(t_f - t_i)}$ can be written as $\mathcal{A} = (\tau_i/\tau_f)^\mu$, where τ_i and τ_f correspond to t_i and t_f , respectively. We assume the amplification factor is constant when $\tau > \tau_f$. Therefore, the amplification factor as a function with τ is parameterized by

$$\mathcal{A}(\tau) = \begin{cases} 1 & \tau < \tau_i, \\ \left(\frac{\tau_i}{\tau}\right)^\mu & \tau_i \leq \tau \leq \tau_f, \\ \left(\frac{\tau_i}{\tau_f}\right)^\mu & \tau > \tau_f. \end{cases} \quad (17)$$

In practise, we set $\mathcal{A} = 0$ when $\tau < \tau_i$ so that the vacuum contribution is subtracted. For simplicity, we consider that the scalar field perturbation is amplified only at $k = k_*$ (k_* is the pivot scale) and tensor perturbations remain unchanged. Thus the mode functions are given by

$$u_k(\tau) = \mathcal{A}(\tau) u_k^{\text{BD}}(\tau) \delta(\ln k/k_*), \quad (18)$$

$$v_k(\tau) = v_k^{\text{BD}}(\tau). \quad (19)$$

In principle it is straightforward to generalize the delta function to a realistic momentum distribution.

Now let us consider the one-loop contribution to the tensor bispectrum from the bubble diagram in Fig. 1. For the polarization configuration $+++$, the results are

$$\begin{aligned} \langle h_{\mathbf{k}_1}^+(\tau) h_{\mathbf{k}_2}^+(\tau) h_{\mathbf{k}_3}^+(\tau) \rangle'_{2a} &= -\frac{1}{2} \left(\frac{H}{M_{\text{p}}}\right)^6 \Theta_{2-\tilde{k}_1} \bar{w}_{k_1}^{++++} \\ &\times \frac{1}{k_1^3 k_2^3 k_3^3 k_*^4} \int_{x_0}^0 dx' \int_{x_0}^0 dx'' \mathcal{F}(\tilde{k}_1, x') \mathcal{G}(\tilde{k}_2, \tilde{k}_3, x'') \\ &+ 2 \text{ perms}, \end{aligned} \quad (20)$$

$$\begin{aligned} \langle h_{\mathbf{k}_1}^+(\tau) h_{\mathbf{k}_2}^+(\tau) h_{\mathbf{k}_3}^+(\tau) \rangle'_{2b} &= \frac{1}{2} \text{Re} \left(\frac{H}{M_{\text{p}}}\right)^6 \Theta_{2-\tilde{k}_1} \bar{w}_{k_1}^{++++} \\ &\times \frac{1}{k_1^3 k_2^3 k_3^3 k_*^4} \int_{x_0}^0 dx' \int_{x_0}^{\tau'} dx'' \left[\mathcal{F}(-\tilde{k}_1, x') \mathcal{G}(\tilde{k}_2, \tilde{k}_3, x'') \right. \\ &\left. + \mathcal{F}^*(\tilde{k}_1, x'') \mathcal{G}^*(-\tilde{k}_2, -\tilde{k}_3, x') \right] + 2 \text{ perms}, \end{aligned} \quad (21)$$

where $x = k_*\tau$, $\tilde{k}_i = k_i/k_*$, and $\Theta_{2-\tilde{k}_1}$ is the Heaviside step function with the argument $2 - \tilde{k}_1$ that implies the

momentum conservation. Here we have introduced

$$\begin{aligned}
\mathcal{F}(\tilde{k}_1, x) &= \frac{1}{x^2} (1 + i\tilde{k}_1 x)(1 + ix)^2 e^{-i(\tilde{k}_1+2)x} \mathcal{A}(x/k_*)^2, \\
\mathcal{G}(\tilde{k}_2, \tilde{k}_3, x) &= \frac{1}{x^2} (1 - i\tilde{k}_2 x)(1 - i\tilde{k}_3 x)(1 - ix)^2 \\
&\quad \times e^{i(\tilde{k}_2+\tilde{k}_3+2)x} \mathcal{A}(x/k_*)^2, \\
\bar{w}_{k_1}^{+++} &= \frac{-A_{k_1 k_2 k_3}^2 k_T^2 k_*^4 (k_1^2 - 4k_*^2)^2}{512\pi^2 k_1^3 k_2^2 k_3^2}, \tag{22}
\end{aligned}$$

where $A_{k_1 k_2 k_3} \equiv 1/4 \sqrt{k_T(k_T - 2k_3)(k_T - 2k_2)(k_T - 2k_1)}$ is the area of the triangle of sides k_i and $k_T \equiv k_1 + k_2 + k_3$. The detailed derivation of the one-loop contribution from the bubble diagram is given in Appendix A.

The scalar field perturbation is enhanced on sub-horizon scales due to parametric resonance. Without loss of generality, we set the initial time and final time of amplification as $x_i = -100$ and $x_f = -10$, and set the index as $\mu = 2$. This implies that $\delta\chi$ is amplified by a factor of $(x_i/x_f)^\mu = 10^2$ within the horizon. The rescaled shape function $(h_{\mathbf{k}_1}^+ h_{\mathbf{k}_2}^+ h_{\mathbf{k}_3}^+)' (H/M_p)^{-6} k_1^2 k_2^2 k_3^2$ is shown in Fig. 2. We see that the tensor bispectrum peaks in the squeezed configuration. As discussed in Refs. [19, 20], for the power spectrum of tensor perturbations the delta function in (18) violates the causality resulting in the infrared divergence. To overcome such an issue, a log-normal distribution with a finite width Δ is introduced to replace the delta function,

$$\delta(\ln k/k_*) \rightarrow \frac{1}{\sqrt{2\pi}\Delta} e^{-\frac{\ln(k/k_*)^2}{2\Delta^2}}. \tag{23}$$

Although our work is free from this issue, we also consider the tensor bispectrum in the log-normal case. We find that the log-normal function gives the same shape of the bispectrum as the delta function. Compared to the delta function case, the value of the shape function in the squeezed limit is smaller in the log-normal case. The reason is as follows. For the log-normal distribution, as $k \rightarrow 0$, the step function behaves as a linear function of k , resulting in the peak value smaller than one in the delta function case. The full comparison between delta case and log-normal case are shown in Appendix B. Since this work focuses on the shape of the tensor bispectrum, in what follows we shall consider only the delta function.

Similar to the bubble diagram, it is straightforward to calculate the one-loop contribution from the triangle

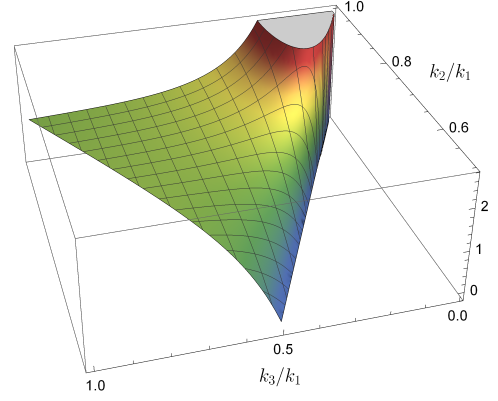


FIG. 2. Rescaled shape function for the +++ polarization from the bubble diagram, where we choose $k_1/k_* = 0.1$. The plot is normalized to unity for equilateral configurations $k_2/k_1 = k_3/k_1 = 1$.

diagram. From Eqs. (14) and (15) we have

$$\begin{aligned}
\langle h_{\mathbf{k}_1}^{s_1}(\tau) h_{\mathbf{k}_2}^{s_2}(\tau) h_{\mathbf{k}_3}^{s_3}(\tau) \rangle'_{3a} &= \left(\frac{H}{M_p} \right)^6 \Theta_{2-\bar{k}_1} \frac{4}{k_1^3 k_2^3 k_3^3 k_*} \\
&\quad \times \left(16A_{k_1 k_2 k_3}^2 - \frac{k_1^2 k_2^2 k_3^2}{k_*^2} \right)^{-1/2} \mathcal{D}^{s_1 s_2 s_3}(k_1, k_2, k_3) \\
&\quad \times \text{Im} \int_{x_0^*}^0 dx' \int_{x_0}^0 dx'' \int_{x_0^*}^{x''} dx''' \mathcal{X}(\tilde{k}_1, x') \\
&\quad \times \left[\mathcal{Y}(\tilde{k}_2, x'') \mathcal{Z}(\tilde{k}_3, x''') + \mathcal{Y}(\tilde{k}_3, x'') \mathcal{Z}(\tilde{k}_2, x''') \right] \\
&\quad + 2 \text{ perms}, \tag{24}
\end{aligned}$$

$$\begin{aligned}
\langle h_{\mathbf{k}_1}^{s_1}(\tau) h_{\mathbf{k}_2}^{s_2}(\tau) h_{\mathbf{k}_3}^{s_3}(\tau) \rangle'_{3b} &= \left(\frac{H}{M_p} \right)^6 \Theta_{2-\bar{k}_1} \frac{4}{k_1^3 k_2^3 k_3^3 k_*} \\
&\quad \times \left(16A_{k_1 k_2 k_3}^2 - \frac{k_1^2 k_2^2 k_3^2}{k_*^2} \right)^{-1/2} \mathcal{D}^{s_1 s_2 s_3}(k_1, k_2, k_3) \\
&\quad \times \text{Im} \int_{x_0^*}^0 dx' \int_{x_0}^0 dx'' \int_{x_0^*}^{x''} dx''' \mathcal{X}(-\tilde{k}_1, x') \\
&\quad \times \left[\mathcal{Y}(\tilde{k}_2, x'') \mathcal{Z}(\tilde{k}_3, x''') + \mathcal{Y}(\tilde{k}_3, x'') \mathcal{Z}(\tilde{k}_2, x''') \right] \\
&\quad + 2 \text{ perms}, \tag{25}
\end{aligned}$$

where

$$\begin{aligned}
\mathcal{X}(k, x) &= \frac{1}{x^2} (1 + ikx)(1 + ix)^2 e^{-i(k+2)x} \mathcal{A}(x/k_*)^2, \\
\mathcal{Y}(k, x) &= \frac{1}{x^2} (1 - ikx)(1 + x^2) e^{ikx} \mathcal{A}(x/k_*)^2, \\
\mathcal{Z}(k, x) &= \frac{1}{x^2} (1 - ikx)(1 - ix)^2 e^{ikx} \mathcal{A}(x/k_*)^2. \tag{26}
\end{aligned}$$

Here $\mathcal{D}^{s_1 s_2 s_3}(k_1, k_2, k_3)$ is the product of projection tensors, which can be written as a compact form for the +++ polarization in the equilateral situation (i.e., $k_1 = k_2 = k_3$).

$$\mathcal{D}^{+++}(k_1, k_1, k_1) = \frac{365k_1^6}{6912} - \frac{61k_1^4 k_*^2}{192} + \frac{9k_1^2 k_*^4}{16} - \frac{k_*^6}{4}.$$

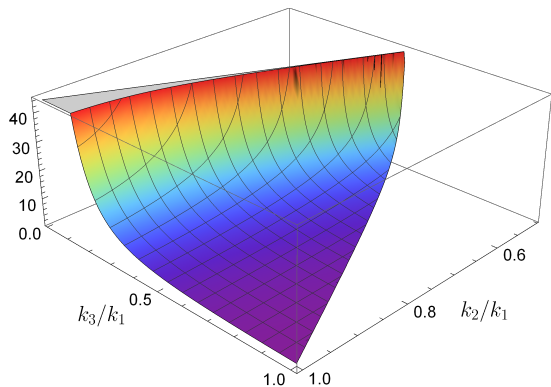


FIG. 3. Rescaled shape function for the $+++$ polarization from the triangle diagram, where we choose $k_1/k_* = 0.1$. The plot is normalized to unity for equilateral configurations $k_2/k_1 = k_3/k_1 = 1$.

In Fig. 3, we display the rescaled shape function for the $+++$ polarization in the case of the triangle diagram. We can see that the tensor bispectrum peaks in the squeezed configuration. Such a result is the same as that obtained in the case of the bubble diagram. The emergence of the squeezed shape appears to resemble the scenario in quasi-single field inflation, where the modes for light isocurvature survive for a long time on super-horizon scales, thereby leading to a quasi-local shape [40, 41]. However, the scalar field perturbation is enhanced on sub-horizon scales in our model. This anomaly could potentially be attributed to the complex interplay between tensor perturbations and scalar field perturbations during inflation. Considering a specific inflationary model would aid in confirming this result. Moreover, we find the peak value of the bispectrum is significantly larger than that from the bubble diagram. The reason is the triangle diagram involves more scalar propagators. Therefore, in this case the contribution from the triangle diagram dominates the one-loop contributions to the tensor bispectrum.

We note that the tensor bispectrum is no longer scale-invariant, due to the presence of a pivot scale k_* . In this context, an additional critical characteristic, besides its shape, is the running of the bispectrum. We take bubble diagram for example. Following the tradition in [41], we show the dependence of the rescaled shape function on the momenta ratio k_2/k_1 and k_3/k_1 , while fixing the perimeter of the momentum triangle k_T in Fig. 4. A outstanding feature is that the tensor bispectrum oscillates in k -space. The underlying physics can be readily understood in terms of generation mechanism. The scalar field perturbation experiences a resonant amplification on sub-horizon scales from τ_i to τ_f , which is similar to resonant non-Gaussianity shown in [42, 43]. Moreover, since we have chosen a specific starting point for resonant amplification, the oscillatory period in k -space is approximately equal to $2\pi/x_i$ which is a constant. Therefore, as k_T increases covering multiple periods, the oscillations become increasingly evident.

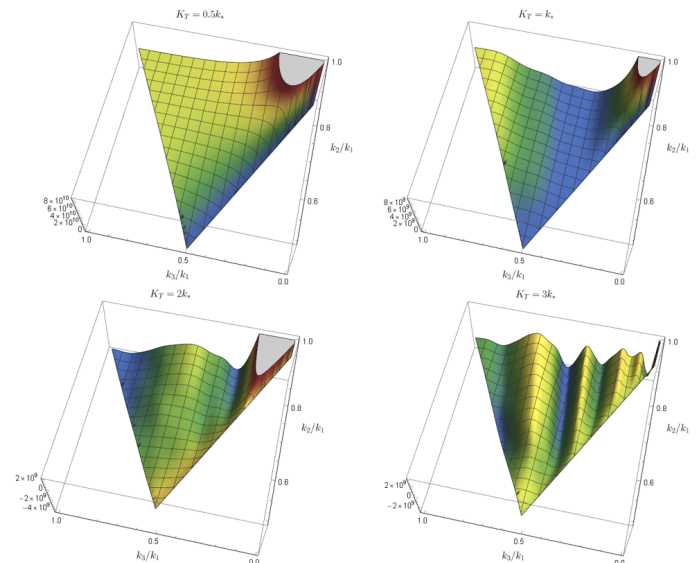


FIG. 4. Rescaled shape function for the $+++$ polarization from the bubble diagram, where we set $k_T = 0.5k_*$, k_* , $2k_*$ and $3k_*$, respectively.

V. CONCLUSIONS AND DISCUSSIONS

We have calculated the tensor bispectrum mediated by an excited scalar field during inflation. We consider the one-loop contributions to the tensor bispectrum from the bubble and triangle Feynman diagrams. In both cases, the bispectrum peaks in the squeezed configuration. After inflation, enhanced scalar perturbations induce another SGWB when re-entering the horizon. The tensor bispectrum of the SGWB is dominated by the equilateral configuration. Hence measurements of the bispectrum provide a potential way to distinguish the SGWBs.

We consider the interaction between tensor perturbations and the spectator scalar field perturbation due to the canonical kinetic term, which is independent of the potential of the scalar field. Moreover, our calculation is based on the exponential growth of the scalar field perturbation only for $k = k_*$ mode. Such an amplification factor can be realized through parametric resonance. For a log-normal momentum distribution around k_* , our conclusions are unchanged.

As an illustration, we show the shape function of the bispectrum only for the $+++$ polarization in Fig. 2 and Fig. 3. Due to parity symmetry, the bispectrum for the $---$ polarization is the same as that for the $+++$ polarization. For the $++-$ and $--+$ polarizations we have checked that the bispectrum takes its maximal value in the squeezed configuration.

It is pointed out that a large amplification of the scalar field perturbation during inflation enables the loop power spectrum to dominate over the tree-level power spectrum in the in-in formalism, indicating the breakdown of the perturbation theory [19, 20, 44]. The necessary condi-

tions for the subdominant loop power spectrum are discussed in Ref. [44]. In our model, the conditions are related to the final value of the amplification factor and thus are assumed to be satisfied.

It is widely held that tensor bispectrum is strongly suppressed at interferometers scales owing to Shapiro time-delay effects associated with the propagation of GWs [23, 24, 45, 46]. A typical counterexample is the flattened configuration of the tensor bispectrum, where phase differences from source to detection are eliminated [47]. Despite the difficulties in measurement, we argue that we theoretically provide a perspective to distinguish the SGWBs generated during inflation from that generated after inflation. Besides, the quadrupolar anisotropy of SGWBs serves as an indirect probe for squeezed tensor non-Gaussianity, which can escape the suppression by propagation effects [48]. Examining the quadrupolar anisotropy in our model may be interesting and we leave it for future work.

Finally, we mention that the SGWB can be sourced by the production of the gauge quanta during inflation with the coupling $\phi F\tilde{F}$ of the pseudoscalar field to the gauge field. The shape of the tensor bispectrum for the $+++$ polarization is very close to equilateral [49]. Although this shape is the same as that of the SGWB induced by enhanced curvature perturbations in the radiation-

dominated era, with the help of parity symmetry, we can distinguish these two SGWBs.

VI. ACKNOWLEDGEMENTS

We thank Xingang Chen, Antonio Riotto, Misao Sasaki and Atsuhisa Ota for comments on the manuscript, and Chao Chen, Zhong-Zhi Xianyu, Yi Wang and Yuhang Zhu for useful discussions. This work is supported in part by the National Key Research and Development Program of China Grant No. 2020YFC2201501, in part by the National Natural Science Foundation of China under Grant No. 12075297 and No. 12235019.

Appendix A: A detailed derivation of the one-loop contribution

In this appendix, I provide a detailed derivation of the one-loop contribution from the bubble and triangle diagrams. The Hamiltonian has both third-order and fourth-order contributions, which results in containing two parts of contributions $\langle \mathcal{O} \rangle_{2a,1}$ and $\langle \mathcal{O} \rangle_{2a,2}$

$$\langle h_{\mathbf{k}_1}^{s_1}(\tau) h_{\mathbf{k}_2}^{s_2}(\tau) h_{\mathbf{k}_3}^{s_3}(\tau) \rangle_{2a,1} = \int_{\tau_0^*}^{\tau} d\tau' \int_{\tau_0}^{\tau} d\tau'' \langle 0 | H_{\text{int}}^{(3)}(\tau') h_{\mathbf{k}_1}^{s_1}(\tau) h_{\mathbf{k}_2}^{s_2}(\tau) h_{\mathbf{k}_3}^{s_3}(\tau) H_{\text{int}}^{(4)}(\tau'') | 0 \rangle, \quad (\text{A1})$$

$$\langle h_{\mathbf{k}_1}^{s_1}(\tau) h_{\mathbf{k}_2}^{s_2}(\tau) h_{\mathbf{k}_3}^{s_3}(\tau) \rangle_{2a,2} = \int_{\tau_0^*}^{\tau} d\tau' \int_{\tau_0}^{\tau} d\tau'' \langle 0 | H_{\text{int}}^{(4)}(\tau') h_{\mathbf{k}_1}^{s_1}(\tau) h_{\mathbf{k}_2}^{s_2}(\tau) h_{\mathbf{k}_3}^{s_3}(\tau) H_{\text{int}}^{(3)}(\tau'') | 0 \rangle. \quad (\text{A2})$$

Based on Eq. (5) and Eq. (6), we can expand the above two equations separately as

$$\begin{aligned} & \langle h_{\mathbf{k}_1}^{s_1}(\tau) h_{\mathbf{k}_2}^{s_2}(\tau) h_{\mathbf{k}_3}^{s_3}(\tau) \rangle_{2a,1} \\ &= -\frac{1}{8} \int_{\tau_0^*}^{\tau} d\tau' a(\tau')^2 \int_{\tau_0}^{\tau} d\tau'' a(\tau'')^2 \prod_{A=1}^7 \left(\int \frac{d^3 p_A}{(2\pi)^3} \right) \\ & \times (2\pi)^3 \delta \left(\sum_{A=1}^3 \mathbf{p}_A \right) (2\pi)^3 \delta \left(\sum_{A=4}^7 \mathbf{p}_A \right) \\ & \times \sum_{s, s_4, s_5} e_{ij}^s(\hat{p}_1) p_{2i} p_{3j} e_{km}^{s_4}(\hat{p}_4) e_{ml}^{s_5}(\hat{p}_5) p_{6k} p_{7l} \\ & \times \langle 0 | h_{\mathbf{p}_1}^{s_1}(\tau') h_{\mathbf{k}_1}^{s_1}(\tau) h_{\mathbf{k}_2}^{s_2}(\tau) h_{\mathbf{k}_3}^{s_3}(\tau) h_{\mathbf{p}_4}^{s_4}(\tau'') h_{\mathbf{p}_5}^{s_5}(\tau'') | 0 \rangle \\ & \times \langle 0 | \delta \chi_{\mathbf{p}_2}(\tau') \delta \chi_{\mathbf{p}_3}(\tau') \delta \chi_{\mathbf{p}_6}(\tau'') \delta \chi_{\mathbf{p}_7}(\tau'') | 0 \rangle. \quad (\text{A3}) \end{aligned}$$

and

$$\begin{aligned} & \langle h_{\mathbf{k}_1}^{s_1}(\tau) h_{\mathbf{k}_2}^{s_2}(\tau) h_{\mathbf{k}_3}^{s_3}(\tau) \rangle_{2a,2} \\ &= -\frac{1}{8} \int_{\tau_0^*}^{\tau} d\tau' a(\tau')^2 \int_{\tau_0}^{\tau} d\tau'' a(\tau'')^2 \prod_{A=1}^7 \left(\int \frac{d^3 p_A}{(2\pi)^3} \right) \\ & \times (2\pi)^3 \delta \left(\sum_{A=1}^3 \mathbf{p}_A \right) (2\pi)^3 \delta \left(\sum_{A=4}^7 \mathbf{p}_A \right) \\ & \times \sum_{s, s_4, s_5} e_{ij}^{s_1}(\hat{p}_1) p_{2i} p_{3j} e_{km}^{s_4}(\hat{p}_4) e_{ml}^{s_5}(\hat{p}_5) p_{6k} p_{7l} \\ & \times \langle 0 | h_{\mathbf{p}_4}^{s_4}(\tau') h_{\mathbf{p}_5}^{s_5}(\tau') h_{\mathbf{k}_1}^{s_1}(\tau) h_{\mathbf{k}_2}^{s_2}(\tau) h_{\mathbf{k}_3}^{s_3}(\tau) h_{\mathbf{p}_1}^s(\tau'') | 0 \rangle \\ & \times \langle 0 | \delta \chi_{\mathbf{p}_6}(\tau') \delta \chi_{\mathbf{p}_7}(\tau') \delta \chi_{\mathbf{p}_2}(\tau'') \delta \chi_{\mathbf{p}_3}(\tau'') | 0 \rangle. \quad (\text{A4}) \end{aligned}$$

We only consider connected graphs, and Eq. (A3) can be simplified as

$$\begin{aligned}
& \langle h_{\mathbf{k}_1}^{s_1}(\tau) h_{\mathbf{k}_2}^{s_2}(\tau) h_{\mathbf{k}_3}^{s_3}(\tau) \rangle_{2a,1} \\
&= -\frac{1}{2} (2\pi)^3 \delta(\mathbf{k}_1 + \mathbf{k}_2 + \mathbf{k}_3) \int_{\tau_0^*}^{\tau} d\tau' a(\tau')^2 \int_{\tau_0}^{\tau} d\tau'' a(\tau'')^2 \\
&\quad \times \prod_{A=2}^3 \left(\int \frac{d^3 p_A}{(2\pi)^3} \right) (2\pi)^3 \delta \left(\sum_{A=2}^3 \mathbf{p}_A - \mathbf{k}_1 \right) \\
&\quad \times e_{ij}^{s_1^*}(\hat{k}_1) p_{2i} p_{3j} e_{km}^{s_2^*}(\hat{k}_2) e_{ml}^{s_3^*}(\hat{k}_3) p_{2k} p_{3l} v_{k_1}^*(\tau) v_{k_2}(\tau) v_{k_3}(\tau) \\
&\quad \times v_{k_1}(\tau') u_{p_2}(\tau') u_{p_3}(\tau') v_{k_2}^*(\tau'') v_{k_3}^*(\tau'') u_{p_2}^*(\tau'') u_{p_3}^*(\tau'') \\
&\quad + 2 \text{ perms.} \tag{A5}
\end{aligned}$$

Similarly, Eq. (A4) is simplified as

$$\begin{aligned}
& \langle h_{\mathbf{k}_1}^{s_1}(\tau) h_{\mathbf{k}_2}^{s_2}(\tau) h_{\mathbf{k}_3}^{s_3}(\tau) \rangle_{2a,2} \\
&= -\frac{1}{2} (2\pi)^3 \delta(\mathbf{k}_1 + \mathbf{k}_2 + \mathbf{k}_3) \int_{\tau_0^*}^{\tau} d\tau' a(\tau')^2 \int_{\tau_0}^{\tau} d\tau'' a(\tau'')^2 \\
&\quad \times \prod_{A=2}^3 \left(\int \frac{d^3 p_A}{(2\pi)^3} \right) (2\pi)^3 \delta \left(\sum_{A=2}^3 \mathbf{p}_A - \mathbf{k}_1 \right) \\
&\quad \times e_{ij}^{s_1^*}(\hat{k}_1) p_{2i} p_{3j} e_{km}^{s_2^*}(\hat{k}_2) e_{ml}^{s_3^*}(\hat{k}_3) p_{2k} p_{3l} v_{k_2}^*(\tau) v_{k_3}^*(\tau) v_{k_1}(\tau) \\
&\quad \times v_{k_2}(\tau') v_{k_3}(\tau') u_{p_2}(\tau') u_{p_3}(\tau') v_{k_1}^*(\tau'') u_{p_2}^*(\tau'') u_{p_3}^*(\tau'') \\
&\quad + 2 \text{ perms.} \tag{A6}
\end{aligned}$$

Note that after exchanging τ' and τ'' , Eq. (A5) and Eq. (A6) are conjugate to each other. Therefore,

$$\langle h_{\mathbf{k}_1}^{s_1}(\tau) h_{\mathbf{k}_2}^{s_2}(\tau) h_{\mathbf{k}_3}^{s_3}(\tau) \rangle_{2a} = 2\text{Re} \langle h_{\mathbf{k}_1}^{s_1}(\tau) h_{\mathbf{k}_2}^{s_2}(\tau) h_{\mathbf{k}_3}^{s_3}(\tau) \rangle_{2a,1}. \tag{A7}$$

Then, we deal with the polarization tensor and momentum integral parts. Due to the conservation of momentum and without losing generality, we can fix all k_i in the (x, z) plane. Such vector triangles can be constructed as

$$\begin{aligned}
\mathbf{k}_1 &= k_1(0, 0, 1), \\
\mathbf{k}_2 &= k_2(\sin \theta, 0, \cos \theta), \\
\mathbf{k}_3 &= k_3(\sin \phi, 0, \cos \phi), \tag{A8}
\end{aligned}$$

where $\sin \theta = \lambda/2k_1k_2$, $\cos \theta = (k_3^2 - k_1^2 - k_2^2)/2k_1k_2$, $\sin \phi = -\lambda/2k_1k_3$, $\cos \phi = (k_2^2 - k_3^2 - k_1^2)/2k_1k_3$, with $\lambda = \sqrt{2k_1^2k_2^2 + 2k_2^2k_3^2 + 2k_3^2k_1^2 - k_1^4 - k_2^4 - k_3^4}$. Polarization tensors are as follows

$$e_{ij}^{s_1}(\hat{k}_1) \equiv \frac{1}{2} \begin{pmatrix} 1 & is_1 & 0 \\ is_1 & -1 & 0 \\ 0 & 0 & 0 \end{pmatrix}, \tag{A9}$$

$$e_{ij}^{s_2}(\hat{k}_2) \equiv \frac{1}{2} \begin{pmatrix} \cos^2 \theta & -is_2 \cos \theta & -is_2 \sin \theta \cos \theta \\ is_2 \cos \theta & -1 & -is_2 \sin \theta \\ -is_2 \sin \theta \cos \theta & -is_2 \sin \theta & \sin^2 \theta \end{pmatrix}, \tag{A10}$$

$$e_{ij}^{s_3}(\hat{k}_3) \equiv \frac{1}{2} \begin{pmatrix} \cos^2 \phi & -is_3 \cos \phi & is_3 \sin \phi \cos \phi \\ -is_3 \cos \phi & -1 & -is_3 \sin \phi \\ -is_3 \sin \phi \cos \phi & -is_3 \sin \phi & \sin^2 \phi \end{pmatrix}, \tag{A11}$$

Because of the independence of the angle in Eq. (A5), we have

$$\begin{aligned}
& \int \frac{d^3 p_2 d^3 p_3}{(2\pi)^6} (2\pi)^3 \delta(\mathbf{k}_1 - \mathbf{p}_2 - \mathbf{p}_3) \\
&= \frac{1}{(2\pi)^2 k_1} \int_0^\infty dp_2 \int_{|p_2 - k_1|}^{p_2 + k_1} dp_3 p_2 p_3. \tag{A12}
\end{aligned}$$

Note that $\mathbf{p}_A = p_A(\sin \theta_A \cos \phi_A, \sin \theta_A \sin \phi_A, \cos \theta_A)$, combining Eq. (A5) and Eqs. (A8)-(A12), we obtain

$$\begin{aligned}
& \int \frac{d^3 p_2 d^3 p_3}{(2\pi)^6} (2\pi)^3 \delta(\mathbf{p}_2 + \mathbf{p}_3 - \mathbf{k}_1) e_{ij}^{s_1^*}(\hat{k}_1) p_{2i} p_{3j} e_{km}^{s_2^*}(\hat{k}_2) \\
&\quad \times e_{ml}^{s_3^*}(\hat{k}_3) (p_{2k} p_{3l} + p_{3k} p_{2l}) f(p_2, p_3) \\
&= \int_0^\infty dp_2 \int_{|p_2 - k_1|}^{p_2 + k_1} dp_3 w_{k_1}^{s_1 s_2 s_3} f(p_2, p_3). \tag{A13}
\end{aligned}$$

where

$$w_{k_1}^{s_1 s_2 s_3} = \frac{A_{k_1 p_2 p_3}^2 k_T^2 p_2 p_3 A_{k_1 p_2 p_3}^4}{2\pi^2 k_1^7 k_2^2 k_3^2}. \tag{A14}$$

$A_{k_1 p_2 p_3}$ refers to the area of the triangle enclosed by k_1 , p_2 and p_3 .

Then we apply the mode function Eq. (18) and Eq. (19) to perform the momentum integration. The calculation is straightforward and the result (for +++ polarization) is

$$\begin{aligned}
& \langle h_{\mathbf{k}_1}^+(\tau) h_{\mathbf{k}_2}^+(\tau) h_{\mathbf{k}_3}^+(\tau) \rangle'_{2a} = -\frac{1}{2} \left(\frac{H}{M_p} \right)^6 \Theta_{2-\tilde{k}_1} \bar{w}_{k_1}^{++++} \\
&\quad \times \frac{1}{k_1^3 k_2^3 k_3^4} \int_{x_0}^0 dx' \int_{x_0}^0 dx'' \mathcal{F}(\tilde{k}_1, x') \mathcal{G}(\tilde{k}_2, \tilde{k}_3, x'') \\
&\quad + 2 \text{ perms,} \tag{A15}
\end{aligned}$$

which is the same as Eq. (20). Note that the definition of $w_{k_1}^{s_1 s_2 s_3}$ is different from $\bar{w}_{k_1}^{s_1 s_2 s_3}$ in Eq. (20). We omit the derivation of $\langle \mathcal{O} \rangle_{2b}$ due to the similarity of calculations.

Now we consider the one-loop contribution from the triangle diagram. Taking $\langle \mathcal{O} \rangle_{3a}$ as an example,

$$\begin{aligned}
& \langle h_{\mathbf{k}_1}^{s_1}(\tau) h_{\mathbf{k}_2}^{s_2}(\tau) h_{\mathbf{k}_3}^{s_3}(\tau) \rangle_{3a} \\
&= \frac{1}{4} \text{Im} \int_{\tau_0^*}^{\tau} d\tau' a^2(\tau') \int_{\tau_0}^{\tau} d\tau'' a^2(\tau'') \int_{\tau_0}^{\tau''} d\tau''' a^2(\tau''') \\
&\quad \prod_{A=1}^9 \left(\int \frac{d^3 p_A}{(2\pi)^3} \right) (2\pi)^9 \delta \left(\sum_{A=1}^3 \mathbf{p}_A \right) \delta \left(\sum_{A=4}^6 \mathbf{p}_A \right) \delta \left(\sum_{A=7}^9 \mathbf{p}_A \right) \\
&\quad \times \sum_{s, s_4, s_7} e_{ij}^{s_1}(\hat{p}_1) p_{2i} p_{3j} e_{kl}^{s_4}(\hat{p}_4) p_{5k} p_{6l} e_{mn}^{s_7}(\hat{p}_7) p_{8m} p_{9n} \\
&\quad \times \langle 0 | h_{\mathbf{p}_1}^{s_1}(\tau) h_{\mathbf{k}_1}^{s_1}(\tau) h_{\mathbf{k}_2}^{s_2}(\tau) h_{\mathbf{k}_3}^{s_3}(\tau) h_{\mathbf{p}_4}^{s_4}(\tau'') h_{\mathbf{p}_7}^{s_7}(\tau''') | 0 \rangle \\
&\quad \times \langle 0 | \delta\chi_{\mathbf{p}_2}(\tau') \delta\chi_{\mathbf{p}_3}(\tau') \delta\chi_{\mathbf{p}_5}(\tau'') \delta\chi_{\mathbf{p}_6}(\tau'') \delta\chi_{\mathbf{p}_8}(\tau''') \delta\chi_{\mathbf{p}_9}(\tau''') | 0 \rangle, \tag{A16}
\end{aligned}$$

Because the scalar field perturbation is amplified only at $k = k_*$,

$$\begin{aligned} \langle h_{\mathbf{k}_1}^{s_1}(\tau) h_{\mathbf{k}_2}^{s_2}(\tau) h_{\mathbf{k}_3}^{s_3}(\tau) \rangle_{3a} &= 2\text{Im}\delta(\mathbf{k}_1 + \mathbf{k}_2 + \mathbf{k}_3) p_*^3 \int_{\tau_0^*}^{\tau} d\tau' a^2(\tau') \int_{\tau_0}^{\tau} d\tau'' a^2(\tau'') \int_{\tau_0}^{\tau''} d\tau''' a^2(\tau''') \\ &\int_0^\infty dp_3 p_3^2 \int_{-1}^1 d\cos\theta \int_0^{2\pi} d\phi e^{i s_1^* \hat{k}_1} p_{2i} p_{3j} e^{i s_2^* \hat{k}_2} p_{2k} p_{2l} e^{i s_3^* \hat{k}_3} p_{3m} p_{3n} v_{k_1}^*(\tau) v_{k_2}(\tau) v_{k_3}(\tau) v_{k_1}(\tau') \\ &u_{p_*}^2(\tau') |u_{p_*}|^2(\tau'') (u_{p_*}^*)^2(\tau''') (v_{k_2}^*(\tau'') v_{k_3}^*(\tau''') + v_{k_3}^*(\tau'') v_{k_2}^*(\tau''')) \\ &\delta(p_3 - p_*) \delta(|\mathbf{p}_3 - \mathbf{k}_1| - p_*) \delta(|\mathbf{p}_3 + \mathbf{k}_3| - p_*) + 2 \text{ perms.} \quad (\text{A17}) \end{aligned}$$

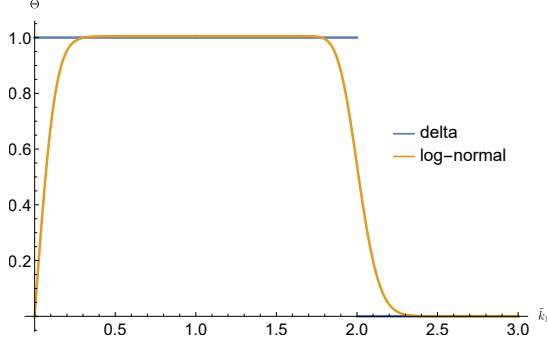


FIG. 5. Step function corresponding to delta distribution and log-normal distribution, respectively.

we integrate out momentum and find that the integral has support at the two points

$$\mathbf{p}_3 = k_1 \left(\frac{-k_1^2 + k_2^2 + k_3^2}{8 A_{k_1 k_2 k_3}}, \pm \sqrt{\frac{16 A_{k_1 k_2 k_3}^2 k_*^2 - k_1^2 k_2^2 k_3^2}{4 A_{k_1 k_2 k_3} k_1}}, \frac{1}{2} \right). \quad (\text{A18})$$

The following calculation is similar to the bubble diagram, so we are not prepared to elaborate on details (so are $\langle \mathcal{O} \rangle_{3b}$). We can see that the above derivation is lengthy and complex. A more elegant and systematic method to compute the correlation functions is the diagrammatic method based on path integral, which provides an equivalent description to canonical in-in formalism [50].

Appendix B: Shape functions under different momentum distributions

In this appendix, we show the shape functions from the bubble diagram in both delta distribution and log-normal distribution.

In log-normal case, from Eq. (23), we obtain [20]

$$f^{\text{LN}}(p_2, p_3) = \frac{e^{-\frac{[\ln(p_2/p_*)]^2 + [\ln(p_3/p_*)]^2}{2\Delta^2}}}{2\pi\Delta^2} f(p_*, p_*). \quad (\text{B1})$$

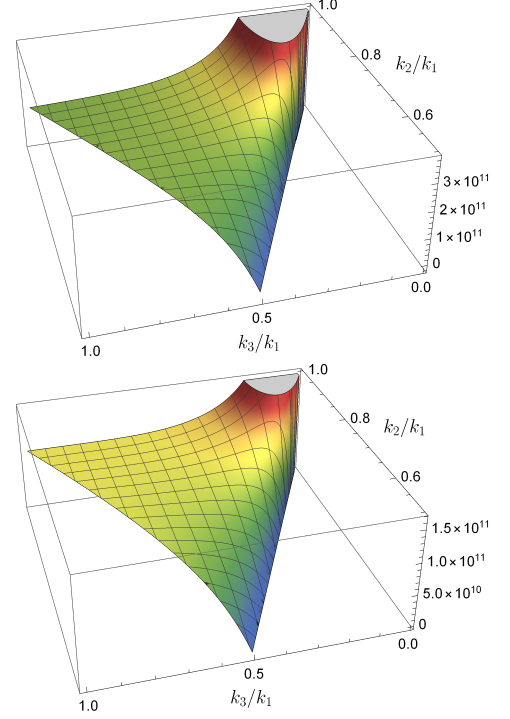


FIG. 6. Rescaled shape functions corresponding to different momentum distributions for the +++ polarization from the bubble diagram, where we choose $k_1/k_* = 0.1$ and $\Delta = 0.1$. Top: delta distribution. Down: log-normal distribution.

we can integrate out one of the momenta, and the remaining integral gives a step function characterized by width Δ

$$\Theta_{2-\tilde{k}_1}^\Delta \equiv \frac{e^{\Delta^2/2}}{2} \left[\text{erf} \left(\frac{\Delta^2 - \ln(|1 - \tilde{k}_1|)}{\sqrt{2}\Delta} \right) - \text{erf} \left(\frac{\Delta^2 - \ln(1 + \tilde{k}_1)}{\sqrt{2}\Delta} \right) \right]. \quad (\text{B2})$$

So the main difference between delta and log-normal distribution is $\Theta_{2-\tilde{k}_1} \rightarrow \Theta_{2-\tilde{k}_1}^\Delta$. Step functions correspond-

ing to delta distribution and log-normal distribution are illustrated in Fig. 5. We find that $\Theta_{2-\tilde{k}_1}^\Delta$ deviates significantly from 1 when k approaches zero. Actually, it behaves as a linear function of k_1 . The same conclusion applies to the other two polarization configurations. The shape functions under two different momentum distributions are shown in Fig. 6. We can see that the peak

value of the shape function in log-normal distribution is smaller than one in the delta case. Meanwhile, the rescaled shape function corresponding to delta distribution $\propto \tilde{k}_1^{-4}$, thus, the configuration of the tensor bispectrum does not change with the momentum distribution, and the squeezed configuration clearly dominates.

-
- [1] G. Agazie *et al.* (NANOGrav), *Astrophys. J. Lett.* **951**, L9 (2023), arXiv:2306.16217 [astro-ph.HE].
- [2] G. Agazie *et al.* (NANOGrav), *Astrophys. J. Lett.* **951**, L8 (2023), arXiv:2306.16213 [astro-ph.HE].
- [3] A. Zic *et al.*, (2023), arXiv:2306.16230 [astro-ph.HE].
- [4] D. J. Reardon *et al.*, *Astrophys. J. Lett.* **951**, L6 (2023), arXiv:2306.16215 [astro-ph.HE].
- [5] J. Antoniadis *et al.* (EPTA, InPTA:), *Astron. Astrophys.* **678**, A50 (2023), arXiv:2306.16214 [astro-ph.HE].
- [6] J. Antoniadis *et al.* (EPTA), *Astron. Astrophys.* **678**, A48 (2023), arXiv:2306.16224 [astro-ph.HE].
- [7] H. Xu *et al.*, *Res. Astron. Astrophys.* **23**, 075024 (2023), arXiv:2306.16216 [astro-ph.HE].
- [8] A. Afzal *et al.* (NANOGrav), *Astrophys. J. Lett.* **951**, L11 (2023), arXiv:2306.16219 [astro-ph.HE].
- [9] Y.-F. Cai, X. Tong, D.-G. Wang, and S.-F. Yan, *Phys. Rev. Lett.* **121**, 081306 (2018), arXiv:1805.03639 [astro-ph.CO].
- [10] Y.-F. Cai, C. Chen, X. Tong, D.-G. Wang, and S.-F. Yan, *Phys. Rev. D* **100**, 043518 (2019), arXiv:1902.08187 [astro-ph.CO].
- [11] R.-G. Cai, Z.-K. Guo, J. Liu, L. Liu, and X.-Y. Yang, *JCAP* **06**, 013 (2020), arXiv:1912.10437 [astro-ph.CO].
- [12] Z. Zhou, J. Jiang, Y.-F. Cai, M. Sasaki, and S. Pi, *Phys. Rev. D* **102**, 103527 (2020), arXiv:2010.03537 [astro-ph.CO].
- [13] Z.-Z. Peng, C. Fu, J. Liu, Z.-K. Guo, and R.-G. Cai, *JCAP* **10**, 050 (2021), arXiv:2106.11816 [astro-ph.CO].
- [14] R.-G. Cai, C. Chen, and C. Fu, *Phys. Rev. D* **104**, 083537 (2021), arXiv:2108.03422 [astro-ph.CO].
- [15] K. Inomata, *Phys. Rev. D* **106**, 043533 (2022), arXiv:2203.04974 [astro-ph.CO].
- [16] J. Fumagalli, G. A. Palma, S. Renaux-Petel, S. Sypsas, L. T. Witkowski, and C. Zenteno, *JHEP* **03**, 196 (2022), arXiv:2111.14664 [astro-ph.CO].
- [17] J. M. Maldacena, *JHEP* **05**, 013 (2003), arXiv:astro-ph/0210603.
- [18] S. Weinberg, *Phys. Rev. D* **72**, 043514 (2005), arXiv:hep-th/0506236.
- [19] A. Ota, M. Sasaki, and Y. Wang, *Mod. Phys. Lett. A* **38**, 2350063 (2023), arXiv:2209.02272 [astro-ph.CO].
- [20] A. Ota, M. Sasaki, and Y. Wang, *Phys. Rev. D* **108**, 043542 (2023), arXiv:2211.12766 [astro-ph.CO].
- [21] J. M. Maldacena and G. L. Pimentel, *JHEP* **09**, 045 (2011), arXiv:1104.2846 [hep-th].
- [22] X. Gao, T. Kobayashi, M. Yamaguchi, and J. Yokoyama, *Phys. Rev. Lett.* **107**, 211301 (2011), arXiv:1108.3513 [astro-ph.CO].
- [23] N. Bartolo, V. De Luca, G. Franciolini, A. Lewis, M. Peloso, and A. Riotto, *Phys. Rev. Lett.* **122**, 211301 (2019), arXiv:1810.12218 [astro-ph.CO].
- [24] N. Bartolo, V. De Luca, G. Franciolini, M. Peloso, D. Racco, and A. Riotto, *Phys. Rev. D* **99**, 103521 (2019), arXiv:1810.12224 [astro-ph.CO].
- [25] E. Dimastrogiovanni, M. Fasiello, G. Tasinato, and D. Wands, *JCAP* **02**, 008 (2019), arXiv:1810.08866 [astro-ph.CO].
- [26] G. Goon, K. Hinterbichler, A. Joyce, and M. Trodden, *JHEP* **10**, 182 (2019), arXiv:1812.07571 [hep-th].
- [27] O. Ozsoy, M. Mylova, S. Parameswaran, C. Powell, G. Tasinato, and I. Zavala, *JCAP* **09**, 036 (2019), arXiv:1902.04976 [hep-th].
- [28] T. Fujita, S. Mizuno, and S. Mukohyama, *JCAP* **01**, 023 (2020), arXiv:1909.07563 [astro-ph.CO].
- [29] X. Gao, T. Kobayashi, M. Shiraishi, M. Yamaguchi, J. Yokoyama, and S. Yokoyama, *PTEP* **2013**, 053E03 (2013), arXiv:1207.0588 [astro-ph.CO].
- [30] S. Choudhury and S. Pal, *Eur. Phys. J. C* **75**, 241 (2015), arXiv:1210.4478 [hep-th].
- [31] Y. Huang, A. Wang, R. Yousefi, and T. Zhu, *Phys. Rev. D* **88**, 023523 (2013), arXiv:1304.1556 [hep-th].
- [32] S. Kanno and M. Sasaki, *JHEP* **08**, 210 (2022), arXiv:2206.03667 [hep-th].
- [33] J.-O. Gong, M. Mylova, and M. Sasaki, *JHEP* **10**, 140 (2023), arXiv:2303.05178 [hep-th].
- [34] A. Agrawal, T. Fujita, and E. Komatsu, *Phys. Rev. D* **97**, 103526 (2018), arXiv:1707.03023 [astro-ph.CO].
- [35] A. Agrawal, T. Fujita, and E. Komatsu, *JCAP* **06**, 027 (2018), arXiv:1802.09284 [astro-ph.CO].
- [36] A. Naskar and S. Pal, *Phys. Rev. D* **98**, 083520 (2018), arXiv:1806.08178 [astro-ph.CO].
- [37] A. Naskar and S. Pal, *Eur. Phys. J. C* **80**, 1158 (2020), arXiv:1906.08558 [astro-ph.CO].
- [38] L. Bordin and G. Cabass, *JCAP* **07**, 014 (2020), arXiv:2004.00619 [astro-ph.CO].
- [39] G. Cabass, D. Stefanyshyn, J. Supel, and A. Thavanesan, *JHEP* **10**, 154 (2022), arXiv:2209.00677 [hep-th].
- [40] X. Chen and Y. Wang, *JCAP* **04**, 027 (2010), arXiv:0911.3380 [hep-th].
- [41] X. Chen, *Adv. Astron.* **2010**, 638979 (2010), arXiv:1002.1416 [astro-ph.CO].
- [42] X. Chen, R. Easther, and E. A. Lim, *JCAP* **04**, 010 (2008), arXiv:0801.3295 [astro-ph].
- [43] R. Flauger and E. Pajer, *JCAP* **01**, 017 (2011), arXiv:1002.0833 [hep-th].
- [44] K. Inomata, M. Braglia, X. Chen, and S. Renaux-Petel, *JCAP* **04**, 011 (2023), [Erratum: *JCAP* **09**, E01 (2023)], arXiv:2211.02586 [astro-ph.CO].
- [45] P. Adshead and E. A. Lim, *Phys. Rev. D* **82**, 024023 (2010), arXiv:0912.1615 [astro-ph.CO].
- [46] A. Kehagias and A. Riotto, (2024), arXiv:2401.10680 [gr-qc].
- [47] C. Powell and G. Tasinato, *JCAP* **01**, 017 (2020), arXiv:1910.04758 [gr-qc].

- [48] E. Dimastrogiovanni, M. Fasiello, and G. Tasinato, *Phys. Rev. Lett.* **124**, 061302 (2020), [arXiv:1906.07204 \[astro-ph.CO\]](#).
- [49] J. L. Cook and L. Sorbo, *JCAP* **11**, 047 (2013), [arXiv:1307.7077 \[astro-ph.CO\]](#).
- [50] X. Chen, Y. Wang, and Z.-Z. Xianyu, *JCAP* **12**, 006 (2017), [arXiv:1703.10166 \[hep-th\]](#).